EUROPEAN FUSION DEVELOPMENT AGREEMENT

EFDA–JET–PR(04)31

T.J.J. Tala, F. Imbeaux, V.V. Parail, C. Bourdelle, G. Corrigan, C. Garbet,
D.J. Heading, X. Litaudon, P.I. Strand, J. Weiland and JET-EFDA Contributors

Fully Predictive Transport Simulations of ITB Plasmas in JET, JT-60U and DIII-D

Fully Predictive Transport Simulations of ITB Plasmas in JET, JT-60U and DIII-D

T.J.J. Tala[1], F. Imbeaux[2], V.V. Parail[3], C. Bourdelle[2], G. Corrigan[2], C. Garbet[2], D.J. Heading[3], X. Litaudon[2], P.I. Strand[4], J. Weiland[4]
and JET-EFDA Contributors[*]

[1]EURATOM-Tekes Association, VTT Processes, FIN-02044 VTT, Finland
[2]Association EURATOM-CEA, CEA, CEA-DSM-DRFC Cadarache, 13108, St Paul lez Durance, France
[3]EURATOM/UKAEA Fusion Association, Culham Science Centre, Abingdon, Oxon. OX14 3DB, UK
[4]Association EURATOM-VR, Chalmers University of Technology, Gothenburg, Sweden
** See annex of J. Pamela et al, "Overview of Recent JET Results and Future Perspectives", Fusion Energy 2000 (Proc. 18th Int. Conf. Sorrento, 2000), IAEA, Vienna (2001).*

Preprint of Paper to be submitted for publication in Nuclear Fusion

ABSTRACT

For the first time, the predictive capabilities of the mixed Bohm/GyroBohm, Weiland and 'retuned' GLF23 transport models are investigated with discharges from the ITPA ITB database by fully predictive transport simulations. A range of plasma conditions is examined for JET, JT-60U and DIII-D discharges with ITBs. Fully predictive transport simulations show that the predictions with the Bohm/GyroBohm model agree very well with experimental results from JET and JT-60U. This indicates the importance of the interplay between the magnetic shear and $\omega_{\mathrm{E}\times\mathrm{B}}$ flow shear in ITB formation. In order to achieve a good agreement in DIII-D, the α-stabilisation had to be included into the model, showing the significant role played by the α-stabilisation in governing the physics of the ITBs. The Weiland and GLF23 transport models show only limited agreement between the model predictions and experimental results. The Weiland model fails to form a clear ITB in any of the three tokamaks, the main reason being the oversize growth rates of ITG and TEM. The growth rates exceed significantly the $\omega_{\mathrm{E}\times\mathrm{B}}$ shearing rates and the growth rates calculated with the gyrokinetic code KINEZERO. The average temperatures and density predicted by the Weiland model are typically in fair agreement with experiments. The GLF23 model often predicts the ITB, but its radial location is too far inside the plasma. This leads to strongly underestimated central temperatures. The heat transport outside the ITB is very well reproduced by the GLF23 transport model. The discharges modelled here are the same as studied with the gyrokinetic flux tube code KINEZERO by C. Bourdelle et al. in this journal.

1. INTRODUCTION

The accuracy of predictive transport modelling in plasmas with Internal Transport Barriers (ITBs) is not as good as that in the standard ELMy H-mode scenario. This stems mainly from the fact that the ITB formation mechanisms are not yet fully understood [1, 2]. In addition, small differences in some plasma profile may move the discharge or the simulation over the threshold of the micro-instability, causing thus large differences in the predictions due to large changes in the growth rates γ of some micro-instability (c.f. ITB appearence/disappearence). Furthermore, the time dependent, non-stationary nature of the ITB plasmas challenges the transport models to work under different plasma conditions within one simulation, like different q-profiles and temperature and density profiles. Because of this, simplified and not self-consistent approaches are usually employed in predictive modelling of ITBs [3, 4, 5]. In addition, very few attempts of predictive transport modelling of ITBs in the ITPA (International Tokamak Physics Activity) ITB database [6] covering several tokamaks have been carried out. As a consequence, the aim in this work is to consider and assess all the aforementioned three problems — by making and comparing fully predictive, self-consistent transport simulations with several transport models for discharges from three different tokamaks.

The leading candidates for ITB triggering and also governing the physics of the ITBs are the

turbulence suppression by the $\omega_{\mathrm{E}\times\mathrm{B}}$ shearing rate [7, 8, 9, 10], by negative or small magnetic shear [8, 10, 11, 12, 13], by α-stabilisation [11, 14], by a large density gradient [15, 16] and by the rational values of the q-profile [17, 18]. In this work, we have used three different transport models, the mixed Bohm/GyroBohm [8, 19], the Weiland [20, 21] and GLF23 [22, 23], to carry out all the transport simulations. However, none of these transport models includes all the enumerated ITB triggering and physics mechanisms. On the other hand, different transport models emphasise different ITB formation mechanisms more strongly and ignore some of them. Therefore, a success or a failure by some model under certain plasma conditions (for example reversed versus flat q-profile) or in some tokamak provides very important information on the relative importance of $\omega_{\mathrm{E}\times\mathrm{B}}$ flow shear, magnetic shear, α-stabilisation, etc. in ITB formation. It may also reveal some ideas on what quantities to vary in order to control ITBs in an optimum way.

In order to investigate whether the three transport models perform similarly in the ITPA ITB database, three pairs of high performance discharges from JET, JT-60U and DIII-D are selected. Having discharges from three different tokamaks enables us to recognise common and non-common features of ITB formation and dynamics between different tokamaks. More importantly, it is possible to perform a cross-tokamak ITB/transport model validation — a critical step necessary to improve the predictive capability of the ITB plasma scenario in the next step devices. One of the discharges in each pair (each tokamak) has a flat q-profile whereas the other one has a strongly reversed q-profile. This allows the q-profile and magnetic shear dependencies predicted by the transport models to be compared with each other and with experiments on different tokamaks. Ultimately, the goal of this study is to clarify what mechanisms govern the physics of the ITBs and whether the mechanisms are the same in different tokamaks under the same, and also different, plasma conditions.

The accuracy of the predictions by the transport models is evaluated with the statistical analysis between the simulation and experimental results. The main emphasis in the transport model evaluation is on the radial location and strength of the ITB. In addition, the growth rates of the Ion Temperature Gradient (ITG) modes and Trapped Electron Modes (TEMs) calculated by the Weiland transport model are compared with those calculated by the gyrokinetic flux tube code KINEZERO [24]. Also, the growth rates predicted by the Weiland and GLF23 transport models are compared with the $\omega_{\mathrm{E}\times\mathrm{B}}$ shearing rates. A more extensive micro-stability analysis of the same discharges using the ITPA ITB database is performed by C. Bourdelle et al. in this journal [25].

One of the fundamental principles in this work is to make fully predictive transport simulations. The concept of 'full predictability' means that five transport equations, i.e. ion and electron heat transport, main ion particle transport, toroidal momentum and current diffusion equations, are solved. Thus, the simulations yield predictions for T_{i}, T_{e}, n_{i}, v_{ϕ} and q, respectively. Predicting the density is important because the self-consistent interaction of the temperature and density and their gradients is crucial in the calculation of the growth rates of ITG and TEM. In addition, ITB formation is strongly affected by the density gradient [16]. Moreover, the off-diagonal contribu-

tions in the transport matrix, i.e. the density and temperature gradients, may cause heat and particle pinches, respectively, and thus influence the ITB dynamics significantly. In order to improve the reliability of the transport/ITB model and its predictive capability, it is of a paramount importance to solve also the toroidal momentum equation rather than use the experimentally measured value for v_ϕ. This is due to the key role played by v_ϕ in the value of the $\omega_{\mathrm{E}\times\mathrm{B}}$ flow shear (at least with unidirectional NBI). Using the experimental value of v_ϕ would give too strong indications to the ITB model where and when to form the barrier. In addition, this approach would break the 'full predictability' and self-consistency principles adopted in this work. Furthermore, extrapolation of the simulation predictions to next step devices would be less reliable. However, at this point we need to note that the GLF23 transport model is integrated only for energy transport and current diffusion in the CRONOS transport code [26], and thus, the experimental density and toroidal rotation are used for the simulations carried out with this model.

All the necessary input data for the three pairs of discharges from JET, JT-60U and DIII-D are taken from the international multi-tokamak ITB database [6]. The input data includes the geometry, the power deposition profiles, the external current density profiles, torque, Z_{eff} as well as the initial and boundary conditions for the transport equations to be solved. Neo-classical quantities are calculated using the NCLASS transport code [27]. The simulations using the Bohm/GyroBohm and Weiland models are performed with the JETTO transport code [28] and the simulations using GLF23 with the CRONOS transport code [26].

One of the main problems in transport simulations, in particular in the multi-tokamak database and with several transport models, is that the input data and simulation procedures can be treated in various ways. As a consequence, in order to minimise their impact on the modelling results, we try to keep the simulation parameters and procedures as identical as possible — both among the simulations in different tokamaks and with different transport models. Therefore, the same set of numerical simulation parameters, such as time steps, number of grid points, equilibrium calculation, etc., are consistently used and treated in an equal manner. Although time steps and equilibrium are not done exactly in the same way in JETTO and CRONOS, such differences do not induce any significant bias in the kind of comparisons carried out in this study. JETTO and CRONOS transport codes were checked to give very similar results with the same input data when using a simple transport model. Finally, the simulation results are handled equally when analysing the accuracy of the predictions and comparing the goodness of the models.

This paper is structured in the following way. The transport codes JETTO and CRONOS are described in section 2. In addition, a brief description of the transport models (Bohm/GyroBohm, Weiland and GLF23) is given. In section 3, the simulation results from the six modelled discharges are compared with the experiments. The successes and failures of the transport models in reproducing the dynamics of the ITBs are illustrated. Section 4 is devoted to the statistical analysis of the simulation predictions. The prediction accuracy of the transport models is evaluated. Finally, the conclusions with a summary are discussed in section 5.

2. TRANSPORT CODES AND TRANSPORT MODELS

JETTO is one and a half dimensional integrated transport modelling code solving the time-dependent transport equations averaged over the magnetic flux surfaces [28]. There are several options for example for the equilibrium calculation, handling the heating and current drive, boundary conditions etc. in the code. We have always used consistently the same code options, described in more detail below, in all the JETTO simulations performed during this study.

In order to be most consistent between the simulations, the input data from the ITPA ITB database has been used as thoroughly as possible. This makes the comparisons of the simulation predictions between the discharges and tokamaks most 'code and modeller' independent. As a consequence, the external power deposition and driven current density profiles by NBI and ICRH as well as torque and $Z_{\rm eff}$ are taken from the ITB database. In addition, the initial conditions for $n_{\rm e}$, $T_{\rm e}$, $T_{\rm i}$, q and v_ϕ as well as the boundary conditions for the same quantities are taken from the database. The boundary conditions are taken on top of the H-mode pedestal although the simulations are performed from $\rho = 0$ to $\rho = 1.0$ where ρ is the normalised toroidal flux coordinate. The boundary conditions for the current diffusion equation, i.e. the q-profile evolution, is the total plasma current, taken from the database.

The equilibrium is solved with the ESCO equilibrium solver that is inside JETTO. All the necessary quantities (toroidal magnetic field, major and minor radii, ellipticity and triangularity) for the equilibrium reconstruction are read from the ITB database. This simplified approach to construct the equilibrium is used because the exact plasma boundary is not available for all the simulated discharges.

The original semi-empirical Bohm/GyroBohm transport model in JETTO [19] was amended to include an empirical ITB formation condition in Ref. [8]. The empirical ITB formation threshold condition was derived from the experimental JET database with discharges having ITBs with a low positive magnetic shear. Recently, this ITB formation condition was supported in Ref. [29] where also ITB discharges with a negative magnetic shear were used. The set of diffusion coefficients can be written as follows:

$$\chi_{\rm e} = 1.0\chi_{\rm gB} + 2.0\chi_{\rm B} + \chi_{\rm neo-al}, \tag{1}$$

$$\chi_{\rm i} = 0.5\chi_{\rm gB} + 4.0\chi_{\rm B} + \chi_{\rm i}^{\rm neo}, \tag{2}$$

$$D = [0.3 + 0.7\rho]\frac{\chi_{\rm e}\chi_{\rm i}}{\chi_{\rm e} + \chi_{\rm i}}, \tag{3}$$

$$\text{where} \quad \chi_{\rm gB} = 5 \times 10^{-6}\sqrt{T_{\rm e}}\left|\frac{\nabla T_{\rm e}}{B_\phi^2}\right|, \tag{4}$$

$$\chi_{\rm B} = \chi_{\rm B_0} \times H(C_1 + s - C_3\omega_{\rm E\times B}/\gamma_{\rm ITG}) \tag{5}$$

$$\text{with} \quad \chi_{\rm B_0} = 4 \times 10^{-5} R\left|\frac{\nabla(n_{\rm e}T_{\rm e})}{n_{\rm e}B_\phi}\right| q^2 \times \left(\frac{T_{\rm e}(0.8\rho_{\rm max}) - T_{\rm e}(\rho_{\rm max})}{T_{\rm e}(\rho_{\rm max})}\right) \tag{6}$$

$$\text{and} \quad \chi_{\rm neo-al} = \frac{c^2 v_{\rm th}}{\omega_{\rm pe}^2 qR}\epsilon. \tag{7}$$

In equations (4)–(7), $T_{\rm e}$ and $T_{\rm i}$ are the electron and ion temperatures, respectively, $n_{\rm e}$ is the electron density, B_ϕ the toroidal magnetic field, R the major radius, q the safety factor, c the speed of light and $v_{\rm th}$ and $\omega_{\rm pe}$ are the electron thermal velocity and plasma frequency as well as R is the major radius and ϵ the inverse aspect ratio. All the neo-classical transport quantities, such as the neo-classical ion heat conductivity $\chi_{\rm i}^{\rm neo}$, electrical resistivity, bootstrap current, etc., are calculated with NCLASS code [27], which is coupled to JETTO and CRONOS. $\chi_{\rm neo-al}$ term represents transport arising from the Electron Temperature Gradient (ETG) modes and has a similar form to one proposed by Ohkawa [31]. The non-locality in the Bohm transport appears in the last term where ρ is the flux surface label defined by $\rho = \sqrt{\Phi/\pi B_\phi}/a_{\rm eff}$ with $a_{\rm eff}$ being the radius of the circle covering the same area as the elongated plasma. $\rho_{\rm max}$ is the value of ρ at the separatrix in the L-mode and on top of the edge barrier in the H-mode. Φ is the toroidal magnetic flux. All the quantities appearing in Eqs. (1)–(7) are expressed in SI units except the temperatures $T_{\rm e}$ and $T_{\rm i}$ whose unit is eV.

ITBs are introduced with the Heaviside step function multiplying the modified Bohm transport in Eq. (5). The controlling parameter is given by the ITB formation threshold condition found in Ref. [8]. We fixed the empirical constants $C_1 = 0.1$ and $C_3 = 1.0$ because the optimum value for C_1 varies between around 0 and 0.2 and for C_3 between 0.5 and 1.6 among the simulated discharges from each three tokamaks. Inside the argument of the step function, $\omega_{\rm E\times B}$ is the flow shearing rate by Hahm-Burrell [30] and $\gamma_{\rm ITG}$ is a simple approximation of the linear growth rate defined as $\gamma_{\rm ITG} = v_{\rm th,i}/R$ with $v_{\rm th,i}$ being the ion thermal velocity. Mathematically, when the argument in the step function $C_1 + s - C_3\omega_{\rm E\times B}/\gamma_{\rm ITG} = 0$ changes its sign, the ITB either forms ($H(x < 0) = 0$) or collapses ($H(x > 0) = 1$). Physically, when the Bohm-type of anomalous transport $\chi_{\rm B}$ is fully suppressed in Eqs. (1)–(3), the internal transport barrier forms.

The toroidal velocity is calculated from the momentum balance equation similarly to the other transport equations using the torque from the neutral beam injection as the source term. The anomalous toroidal viscosity coefficient is assumed to be equal to the ion heat transport coefficient as in Eq. (2). There is experimental evidence on JET and other tokamaks that in the NB heated plasmas, the toroidal viscosity coefficient coincides with the ion heat diffusion coefficient, both radially (at least inside $r/a = 0.8$) and with time [32]. The poloidal rotation is assumed to be neo-classical and is calculated by NCLASS.

The transport coefficients in JETTO with the implemented Weiland model can be described the following simplified way:

$$\chi_{\rm e} = \chi_{\rm e,weil} + 0.1\chi_{\rm B} + \chi_{\rm neo-al}, \tag{8}$$

$$\chi_{\rm i} = \chi_{\rm i,weil} + 0.1\chi_{\rm B} + \chi_{\rm i}^{\rm neo}, \tag{9}$$

$$D = D_{\rm weil} + 0.1\chi_{\rm B}, \tag{10}$$

where $\chi_{\rm e,weil}$, $\chi_{\rm i,weil}$ and $D_{\rm weil}$ describe the effective transport coefficients from the ITG and TEM turbulence calculated by the Weiland model [20, 21, 33, 34, 35]. The actual diffusion coefficients

calculated by the Weiland model and given to JETTO, include also the off-diagonal terms in the transport matrix. The collisions and electro-magnetic effects are ignored in the simulations performed in this work. The reason for using additional 10% of the actual Bohm transport is to introduce the edge transport outside the core region $\rho > 0.8$ where the Weiland model is not compatible with edge plasma turbulence. This is motivated by the fact that on one hand the diffusion coefficients from the Weiland model are typically small in the edge region due to the absence or small values of ITG and TEM there and on the other hand, 10% of Bohm is negligibly small compared with $\chi_{\mathrm{i,weil}}$ $\chi_{\mathrm{e,weil}}$ in the core region. As a consequence, the edge transport arising for example from the resistive ballooning modes or drift alfven waves is effectively taken into account while the core transport is not biased by transport coming from other sources than those predicted by the Weiland model. As a very important detail, there are no empirical or numerical fitting parameters in the present JETTO implementation of the Weiland model.

The micro-turbulence suppression by the $\omega_{\mathrm{E\times B}}$ shearing rate is implemented in the Weiland model in a heuristic way as follows:

$$\chi_{\mathrm{i,e,weil}} \propto \sum_k \frac{\gamma_k - \omega_{\mathrm{E\times B}}}{k_\perp^2} \times H(\gamma_k - \omega_{\mathrm{E\times B}}) \tag{11}$$

where $H(x)$ is the Heaviside step function, γ_k the characteristic growth rate of mode k (ITG, TEM, ...) and $k_\perp$ is the characteristic perpendicular wave vector. The $\omega_{\mathrm{E\times B}}$ shearing rate is calculated in the same way as with the Bohm/GyroBohm transport model, the viscosity assumed to be equal to the ion heat diffusivity.

The simulations using the GLF23 transport model [22] have been performed in the CRONOS transport code [26], in which the v1.61 'retuned' version of GLF23 has been implemented. The electron and ion temperatures are predicted according to the model while densities and toroidal rotation are fixed to their experimental values. The ion densities (deuterium and carbon) are calculated from the experimental electron density and Z_{eff} profiles, read from the ITPA ITB database. Since the GLF23 model is not relevant for the outer part of the plasma $\rho > 0.8$, the mixed Bohm/GyroBohm model is used for the prediction in this outer region. Also, the ion neoclassical diffusivity is used as a lower bound for the thermal diffusion coefficients, both in ion and electron channel. This prevents numerical instabilities where the GLF23 model predicts an anomalous transport equal to zero. The $\omega_{E\times B}$ shearing rate is calculated inside the GLF23 module, consistently with the profiles provided by CRONOS. α-stabilisation is also taken into account inside the GLF23 model.

3. COMPARISON BETWEEN THE SIMULATION RESULTS AND EXPERIMENTS OF THE DISCHARGES FROM JET, JT-60U AND DIII-D

The selection of the simulated discharges was strongly inspired and encouraged by the International Tokamak Physics Activity (ITPA) group on transport and ITB physics and the earlier work carried out by the group [4]. LINK TO CLARISSE'S WORK! In order to see whether the agree-

ment between the experimental and predicted results by the transport models is consistent in the multi-machine ITB database, two discharges from each tokamak, i.e. JET, JT-60U and DIII-D, were chosen. One of the discharges in each pair has a monotonic or flat q-profile while the other one has a strongly reversed q-profile. This is motivated due to the strong influence of the magnetic shear and q-profile on the dynamics of the ITB. As a consequence, predictive modelling of these three pairs of discharges will reveal firstly the differences in the transport model predictions due to variations in the magnetic shear and q-profile and secondly, the consistency in the prediction capabilities of the models over the multi-machine database. This will further give us indications on the predictive capability of the models in future tokamaks, like in ITER, in the ITB plasma regime. The main plasma parameters for the six simulated discharges are presented in Table 1. The micro-stability analysis of the same discharges is performed in [25].

Table 1: The simulated discharges from the ITPA ITB database.

Tokamak	Pulse No.	B_ϕ [T]	I_p [MA]	P_in [MW]	Reversed q
JET	46664	3.4	3.4	22	no
JET	53521	3.4	2.0	22	yes
JT-60U	34487	3.7	1.5	13	no
JT-60U	39056	3.7	1.3	8	yes
DIII-D	87031	2.1	1.6	9	no
DIII-D	95989	2.1	1.6	5	yes

The fully predictive simulations (n_e, T_e, T_i, q and v_ϕ predicted) for each discharge are performed for the whole time that exists in the ITB database. The shortest time was 0.4 s for JT-60U discharge no. 39056 and the longest one was 10.0 s for JET discharge no. 53521. The maximum length of the simulations is motivated in the ITB regime because the ITB discharges are usually not in steady-state, for example with respect to the q-profile evolution. As a consequence, in order to assess the goodness of the model prediction and model comparison in an optimum way, it is essential to extend the simulations as long in time as possible. This stems from the fact that if the model can sustain an existing ITB, it is not necessarily able to trigger or collapse it. For some pulses (JET), the data cover both the preheating and main heating phases while for other discharges, like the quasi steady-state discharges in JT-60U, the data cover only the high performance phase.

The time evolution of one of the simulated discharges with a monotonic q-profile (pulse no. 87031 in DIII-D) is illustrated in figure 1 (solid curve). The simulation predictions with the Bohm/GyroBohm (dashed), the Weiland (dash-dotted) and GLF23 (dotted) models are also shown. As can be seen, the volume averaged temperatures and density are predicted well by the transport models for this discharge (density is not predicted with GLF23). On the other hand, the reason for showing the time traces for this discharge is that the predicted plasma profiles are the worst for this discharge, for example with respect to the ITB location, among the six simulated pulses. In the coming analysis of the plasma profiles, the instants of the plots have been chosen to be at the

end of the high power phase, i.e. at the end of the simulation. However, in the statistical analysis presented in section 4, all the profiles at each simulated time point from the start until the end of the simulations have been used when calculating the mean and standard deviation of the prediction uncertainties.

Figures 2–4 illustrate the profiles of T_i, T_e, n_e and v_ϕ for the three pairs of discharges from JET, JT-60U and DIII-D in the respective order at the end of each simulation. In JT-60U, the toroidal rotation v_ϕ is replaced with the q-profile because the toroidal velocity almost vanishes due to the balanced NBI although it is predicted similarly to JET and DIII-D discharges. In all the three figures, the label scheme is as follows: the solid curves correspond to the experimental data from the ITPA ITB database, and the dashed, dash-dotted and dotted curves to the simulation predictions by the mixed Bohm/GyroBohm, Weiland and GLF23 transport models, respectively. Also in each figure, the plots on the left-hand side present the data and simulation results for the discharge with a monotonic or flat q-profile and on the right-hand side for the discharge with a reversed q-profile in each tokamak, respectively.

The predictions with the Bohm/GyroBohm model show rather good agreement with experiments for JET discharge no. 46664 (positive shear). Although the ion and electron temperatures are overestimated, the radial location of the ITB and toroidal rotation are almost perfectly matched. On the contrary, the Weiland model exhibits no sign of an ITB and thus underestimates the central ion temperature significantly. Both the Bohm/GyroBohm and Weiland models underestimate the heat transport outside the ITB ($\rho \geq 0.5$) while the density is well reproduced. On the other hand, GLF23 reproduces well the anomalous heat transport outside the ITB, as shown in the temperature profiles. However, it fails to predict the ITB, leading to the strong underestimation of central T_i and T_e.

For JET discharge no. 53521, the Bohm/GyroBohm model predicts the ITB 10 cm too wide, and thus overestimates the ion temperature. There is no clear ITB in the electron temperature profile although the central value agrees well with the experimental one. The Weiland model underestimates the heat transport outside the ITB which leads to the overestimation of T_i and T_e. The largest problems in JET that the Weiland model has are with v_ϕ, which is strongly overestimated in the outer part of the plasma, and with the central T_i. The GLF23 model predicts the location and strength of the ITB well in T_i, and thus the ion temperature is in good agreement with the experiment. Interestingly, the electron heat channel does not show any ITB and consequently, the central electron temperature is significantly underestimated. However, the electron heat transport is again well reproduced outside the ITB.

The agreement between the experimental and simulated data with the Bohm/GyroBohm model is very good also in JT-60U, in particular with respect to the radial location of the ITB. Interestingly, with the positive shear, the model overestimates T_e and n_e whereas with the negative shear, it does quite the opposite while the ion temperature matches the experimental value well in both cases. This could be an indication of the stronger turbulence suppression (for example TEM) with

the negative magnetic shear than predicted by the Bohm/GyroBohm transport model. In neither case does the Weiland model exhibit an ITB nor a good agreement with experiments.

JT-60U pulse no. 39056 has almost a current hole in the centre (q approaching infinity) as shown by the solid curve in figure 3(h). In JETTO, the maximum value of the q-profile must be limited in order to prevent the simulations from crashing. This limit, which is in this case $q_{\max} = 30$, is one reason for the predicted q-profile to deviate from the reconstructed one. There are two reasons why the predicted q-profiles between the two transport models (dashed versus dash-dotted), and also between the experimental one (solid), look so different with each other. Firstly, the bootstrap current is very large (about 65% of the total current) with the prediction of the Bohm/GyroBohm model due to the strong ITB (pressure gradient) and much smaller (about 30% of the total current) with the prediction of the Weiland model with small pressure gradient. Secondly, the lower $T_{\rm e}$ predicted by the Weiland model enhances the current penetration to the centre of the plasma. In all the other five discharges (they do not exhibit a current hole), the agreement between the simulated and experimental q-profile is much better, in particular with the Bohm/gyroBohm model. The agreement depends on the prediction accuracy of the location and strength of the ITB, with the location and strength being directly linked to the location and amount of the driven bootstrap current, respectively.

In DIII-D, the Bohm/GyroBohm model does not predict the shape of $T_{\rm i}$ and $n_{\rm e}$ profiles as well as in JET and JT-60U. In addition, the radial location of the ITB is somewhat overestimated by $\rho \approx 0.15$, which is, as a figure of merit for an ITB model, however, not particularly bad. Furthermore, the model has large difficulties in predicting correctly the shape of the toroidal rotation profile. The disagreements are firstly due to the fact that there is no ITB in the density profile in the experimental data whereas the simulations predict that and secondly, the ion temperature and toroidal rotation profiles peak towards the magnetic axis, not predicted by the model. The qualitative difference in the shape of the experimental plasma profiles ($T_{\rm i}$ and v_ϕ peaking and no ITB in $n_{\rm e}$) between DIII-D and JET or JT-60U indicates that the ITB dynamics and turbulence may be governed by other mechanisms than those in JET and JT-60U. In order to obtain a better consistency in the accuracy of the predictions over the various tokamaks, we will try to include explicitly the role of α-stabilisation (Shafranov shift) in the Bohm/GyroBohm model. The α-stabilisation is not taken into account in the standard Bohm/GyroBohm model, presented in section 2.

The Weiland model fails to reproduce an ITB and the shape of the plasma profiles in either DIII-D pulse. However, transport outside the location of the ITB is better reproduced in DIII-D than in JET or JT-60U. Reproducing the toroidal rotation seems to be again the biggest problem. GLF23 model predicts a clear ITB for pulse no. 87031, but far too close to the centre of the plasma at $t = 1.85$s. However, earlier in the shot at $t = 1.7$s, a broader ITB was predicted. This ITB was in much better agreement with the experiment, but it did not survive and shrank up to the radial location shown in figure 4(a). For pulse no. 95989, some hints of a weak inner ITB appear along the time evolution of the GLF23 simulation, but it does not develop properly. As for JET

discharges, the temperatures are well reproduced outside the ITB ($0.5 < \rho < 0.8$), especially for T_i.

In order to study the possible role of α-stabilisation with the Bohm/GyroBohm model, the ITB formation threshold condition, given in equation (5), had to be modified. At least for trapped electron modes, according to Ref. [36], stabilisation of the growth of the modes is predicted when the condition $3/8 + s - 3/5\alpha < 0$ is fulfilled. In the following approach, we will apply the same stabilisation criterion also to ions. When combining this expression with equation (5), the amended ITB threshold condition takes the following form:

$$\chi_\mathrm{B} = \chi_{\mathrm{B}_0} \times \Theta(C_1 + s - C_3\omega_{\mathrm{E\times B}}/\gamma_\mathrm{ITG} - 3/5\alpha) \tag{12}$$

where α is defined as in MHD, i.e. $\alpha = -2Rq^2\mu_0/B^2 dp/dr$ with p being the pressure and μ_0 the permeability of the vacuum. The numerical constant C_3 was kept in the same value (C_3=1.0) as in equation (5). In order to be as consistent as possible with the old (equation (5)) and new ($3/8 + s - 3/5\alpha < 0$) ITB threshold conditions, the numerical constant C_1 was set to 0.5. This stems roughly from the sum of the original equation (5) where C_1 was equal to 0.1 and the new TEM stabilisation term that requires $C_1 = 3/8$. Effectively, the new ITB condition replaces the constant $C_1 = 0.1$ with $0.5 - 3/5\alpha$.

The effect of the α-stabilisation with the amended ITB threshold condition is illustrated in figure 5 for the two DIII-D discharges. The experimental data (solid curves) and the predictions by the standard Bohm/GyroBohm model (dashed curves) are the same as in figure 4 whereas the dash-dotted lines correspond to the simulations with the amended model with the α-stabilisation. The agreement between the experiments and modelling improves in all respects (except maybe the marginal decrease in T_e) after the inclusion of the α-stabilisation term, for either DIII-D discharge, independently of the difference in the q-profile and magnetic shear. The radial location of the foot of the ITB has moved inwards with respect to the previous simulations, being in much better agreement with the experiment. In addition, the model predicts somewhat stronger peaking towards the axis in T_i as observed in the experiments. Still, the model does not predict the toroidal rotation profile well, in particular with the flat q-profile (pulse no. 87031).

The same simulations, with the α-stabilisation included according to equation (12), were also repeated for JET and JT-60U discharges. Very interestingly, the simulation results between the old and new ITB models were very similar. Only in one case (JET pulse no. 53521), the central ion or electron temperature changed more than 1 keV. In all the four cases, the footpoint of the ITB changed less than $\rho < 0.05$, being closer to the experimental footpoint of the ITB in two cases and further also in two cases than in the simulations without the α-term. Thus, since the ITB shrank radially in DIII-D (approximately by $\rho \approx 0.1$), it indicates that the new ITB threshold condition has larger values around the ITB location than the old one, i.e. $0.5 - 3/5\alpha > 0.1$. On the other hand, in JET and JT-60U including the α-stabilisation did not change significantly the radial location of ITB. Therefore, the comparison of the new and old ITB threshold conditions gives approximately $0.5 - 3/5\alpha \approx 0.1$ in JET and JT-60U. This indicates that the value of α is

stronger in JET and JT-60U than in DIII-D, at least around the ITB, and accordingly α-stabilisation plays a larger role in determining its radial position. A similar conclusion by Bourdelle et al. [25] from the micro-stability analysis stated that α has larger impact on ITBs in JT-60U than in DIII-D. However, from the modelling point of view, taking into account the α-stabilisation improved the simulation predictions of the Bohm/GyroBohm model significantly in DIII-D whereas in JET and JT-60U, the modelling results changed only marginally. This can be interpreted that in JET and JT-60U, the effect of α can be hidden, possibly by coincidense, in the value of constant C_1 while in DIII-D, α must be taken as a separate contributor to the ITB formation threshold condition. In conclusion, a better agreement between the modelling predictions in the multi-machine database is achieved when the α-stabilisation is explicitly taken into account as in equation (12), rather than hidden in constant C_1 as in equation (5).

It is quite solid to state that the Weiland model is not capable of predicting the ITB plasmas satisfactorily in the multi-tokamak database. The overall agreement of the temperature and density profiles is in many cases not so poor, at least for T_e and n_e, but the absence of the ITB justifies the negative statement above. There are probably several reasons for the failure. One of the most obvious reasons is illustrated in figure 6. The linear growth rates presented in figure 6 are shown before the subtraction of the $\omega_{\mathrm{E}\times\mathrm{B}}$ shearing rate. The linear growth rates calculated by the Weiland model exceed the $\omega_{\mathrm{E}\times\mathrm{B}}$ shearing rate by a factor of 2–10, depending on the discharge. In order to trigger an ITB, the $\omega_{\mathrm{E}\times\mathrm{B}}$ flow shear must be multiplied artificially typically by a factor of about 10 even if the ratio $\gamma/\omega_{\mathrm{E}\times\mathrm{B}}$ would be less than 10. This is because the artificially increased shearing rate decreases gradually transport (as shown in equation (11)) which then allows the temperature profiles to steepen, and this further leads to increased growth rates, and to compensate these, the $\omega_{\mathrm{E}\times\mathrm{B}}$ shearing rate needs to be further increased. This seemed to be true at least in JET and DIII-D where the dominant contribution to the $\omega_{\mathrm{E}\times\mathrm{B}}$ flow shear comes from the toroidal rotation due to unidirectional NBI.

However, although the $\omega_{\mathrm{E}\times\mathrm{B}}$ shearing rate is too small to suppress the growth of the micro-turbulence within the ITB, ultimately, the problem in the Weiland model originates from the large, oversize growth rates rather than from the small $\omega_{\mathrm{E}\times\mathrm{B}}$ shearing rate. Oversize growth rates as compared with the $\omega_{\mathrm{E}\times\mathrm{B}}$ shearing rate predicted by the Weiland model in ITB plasmas are recently reported in [37]. As a comparison, the growth rates calculated with the KINEZERO gyro-kinetic code are illustrated in figure 6 by the dotted lines. The growth rates represent the maximum growth rate in the region $k_\theta\rho_\mathrm{i} < 2$ with k_θ being the poloidal wave number of the mode and ρ_i the ion larmor radius. This region is characteristic for the ITG and TEM instabilities. The temperature and density profiles, q, Z_eff and all the needed plasma parameters are taken from the corresponding JETTO simulations with the Weiland model at the same time as the plasma profiles shown in figures 2–4. As can be seen, the growth rates calculated by the Weiland model are systematically larger than those calculated by KINEZERO for all six discharges. They are also larger than predicted by the simple estimate for γ_ITG used in the Bohm/GyroBohm transport model. In JET and JT-60U,

the growth rates predicted by the Weiland model are about a factor of 2 larger than those by predicted KINEZERO whereas in DIII-D, the factor is above 3. In JET, the growth rates predicted by KINEZERO are of the order of the $\omega_{\mathrm{E}\times\mathrm{B}}$ flow shear whereas in DIII-D the $\omega_{\mathrm{E}\times\mathrm{B}}$ shearing rates exceed the growth rates over the whole radius. The large shearing rates in DIII-D are due to the fact that the Weiland model predicts the toroidal rotation profiles poorly. In addition, KINEZERO predicts full stabilisation of ITG/TEM inside ρ = 0.3–0.55 (depending on the pulse) whereas the Weiland model gives significant growth rates up to ρ = 0.1–0.2. According to KINEZERO, with the plasma profiles predicted by the Weiland model, the most contributing micro-instability in the JT-60U plasmas is TEM whereas in DIII-D, the dominant micro-instability is ITG. In JET, both instabilities contribute rather equally to γ. Although the growth rates predicted by the Weiland model were significantly larger than those predicted KINEZERO, the micro-stability analysis with the Weiland model is in qualitative agreement with KINEZERO results, i.e. TEM dominates in JT-60U and ITG in DIII-D while both instabilities are roughly equal in JET. Predicting too high growth rates is actually a generic problem of the fluid models, like the Weiland model, as compared with the kinetic models as the thresholds of the instabilities are too low [38]. A more extensive micro-instability study of the same discharges with KINEZERO using the experimental plasma profiles from the ITPA database is reported in [25].

In the version of the Weiland model used in this work, the Electro-Magnetic (EM) effects and the collisions were switched off. The reason for not having those effects on was that we preferred to use exactly the same model for all the simulations (discharges). However, we could not run all the simulations with them on due to numerical instabilities, in particular in the particle transport. As an example of a simulation with EM effects and collisions switched on, the growth rate γ for DIII-D pulse no. 95989 is shown in figure 6(f) by the dotted line. It looks that including the EM effects and collisions might be a good approach towards forming an ITB, at least in this case because the $\omega_{\mathrm{E}\times\mathrm{B}}$ shearing rate is almost exceeding the growth rate. Another way to improve the predictive capability of the Weiland model would be to modify the effect of the negative and small magnetic shear on the growth of the unstable modes. In the present version, which is the standard version of the model, the impact of the magnetic shear on the growth rates is rather weak. Preliminary results with the modified Weiland model yielded somewhat smaller growth rates leading to profile steepening and a signature of an ITB in regions with a negative or small magnetic shear.

The problems with the GLF23 model are different from those of the Weiland model, as described above. The GLF23 model predicts the ITB (in three of the four simulated discharges), unlike the Weiland model, but the footpoint of the ITB is located too far inside the plasma. As a result, the prediction of the central temperatures is underestimated. This conclusion is quite different from the results obtained by Kinsey et al. in Ref. [39] where an excellent agreement is found on the ITB prediction using GLF23. This paper even studies one shot in common with the present work (i.e. DIII-D 95989, at $t = 0.88$ s), and finds a correct prediction of the ITB. The main difference between the two modelling studies is that we carry out time-dependent simulations of a

discharge over several energy confinement times, while in Ref. [39], GLF23 is used to find a stationary solution at a given time slice. The two procedures would be equivalent if GLF23 was able to reproduce the whole discharge evolution starting from $t = 0.41$ s. But we lose in our simulation the broad ITB quite rapidly during the discharge evolution. Therefore, firstly the q-profile is different from the experimental one at $t = 0.88$ s and secondly, the calculated temperature profiles do not correspond to the stationary solution of the time slice at $t = 0.88$ s. Thus, we deduce from this difference between the two studies that the turbulence stabilisation conditions operating in GLF23 are not robust enough to perform an accurate time-dependent simulation of an ITB discharge. This suggests that some adjustments of the turbulence stabilisation mechanisms are necessary in the model, in view of triggering more easily broader ITBs.

The growth rates predicted by the GLF23 transport model are compared with the $\omega_{\mathrm{E\times B}}$ shearing rates in figure 7. It can be seen that for discharges where the shearing rate exceeds the growth rate (JET pulse no. 53521 and DIII-D pulses 87031 and 95989), GLF23 predicts the ITB at that radius. For the two DIII-D discharges, the growth rate is above, but quite close to the $\omega_{\mathrm{E\times B}}$ shearing rate, in the region $0.2 < \rho < 0.4$. Therefore, the model is close to triggering a wider ITB, which would be in better agreement with the experiment. This occurs but only transiently (e.g. for shot 87031 at t = 1.7 s). As a consequence, the turbulence stabilisation mechanisms in the model might require a small adjustment, although the simulations performed here do not show clearly which one should be amplified (magnetic shear, $\omega_{\mathrm{E\times B}}$ flow shear, α-stabilisation, ...). Nevertheless, a distinctive and remarkable feature of GLF23 is the very good agreement of its temperature predictions outside the ITB. This shows that GLF23 predicts the correct level of anomalous heat transport in the absence a strong local turbulence stabilisation (like ITB).

4. STATISTICAL ANALYSIS OF THE SIMULATION PREDICTIONS

In order to be able to quantify and compare the agreement between the simulation predictions and experiments, a statistical approach to the simulation results must be applied. There are several ways to do it. In this study, we calculate the simulation offsets (mean) and standard deviation with the subtracted offset according to the following equations:

$$m_Y = \sum_{i=1}^{K} \frac{(\sum_{j=1}^{N} Y_j)}{N}/K, \tag{13}$$

$$\sigma_Y^2 = \sum_{i=1}^{K} \left(\frac{\sum_{j=1}^{N} (Y_j - m_{\mathrm{Y,i}})^2}{N} \right)/K, \tag{14}$$

$$\text{where } m_{\mathrm{Y},i} \text{ and } Y_j \text{ are defined as}$$

$$Y_j = (Y_{\mathrm{exp}}(x_j) - Y_{\mathrm{sim}}(x_j))/Y_{\mathrm{sim}}(x_j) \tag{15}$$

$$m_{Y,i} = (\sum_{j=1}^{N} Y_j)/N \text{ for each } i. \tag{16}$$

The inner summation from $j = 1$ to N in equations (13)–(16) is over the radial grid points ($N = 51$) from $\rho = 0.0$ to $\rho = 0.8$ and the outer summation $i = 1$ to K is over evenly distributed K time points within the time interval of the simulation, i.e. the instants where the radial profiles

have been taken. The reason for using $\rho = 0.8$ as the most outer radial point in the statistical analysis is that the data, in particular T_i and v_ϕ, are not very accurate outside that radius. The calculated quantity m_Y symbolises the time averaged modelling offset of the quantity Y, which can be either T_i, T_e, n_e or v_ϕ. The quantity σ_Y^2 stands for the variance between the experimental measurement and the modelling prediction of the quantity Y. What is important in the definition of σ_Y^2 is that the mean offset (error) $m_{\mathrm{Y},i}$ at each time point i is subtracted. This is an elegant way to weigh the agreement of the radial location and the strength of the ITB between the simulation and experiment, rather than emphasising the overall agreement of the actual values of the quantity Y over the radius. $Y_\mathrm{exp}(x_j)$ is the measured value (ITPA database value) of a given quantity at the radial point x_j and $Y_\mathrm{sim}(x_j)$ is the simulated one at the same point. Consequently, m_Y and σ_Y characterise the time averaged modelling offset and the time averaged standard deviation with the subtracted offset, respectively, compared to the measured quantities over the whole duration of the simulation. The prediction offsets are presented in table 2 and the standard deviations in table 3 for all the 6 simulated discharges, illustrated in figures 2–4.

Table 2: The simulation offsets between the experiments and simulations with the Bohm/GyroBohm transport model $m_{\mathrm{Y,B}}$, the Weiland transport model $m_{\mathrm{Y,W}}$ and the GLF23 transport model $m_{\mathrm{Y,G}}$ of the quantity Y.

Tokamak	Pulse No.	$m_{\mathrm{Ti,B}}$	$m_{\mathrm{Ti,W}}$	$m_{\mathrm{Ti,G}}$	$m_{\mathrm{Te,B}}$	$m_{\mathrm{Te,W}}$	$m_{\mathrm{Te,G}}$	$m_{\mathrm{ne,B}}$	$m_{\mathrm{ne,W}}$	$m_{\mathrm{v_\phi,B}}$	$m_{\mathrm{v_\phi,W}}$
JET	46664	-0.11	-0.13	0.36	-0.08	-0.14	0.73	0.12	0.01	0.09	-0.37
JET	53521	-0.15	-0.50	0.08	-0.17	-0.25	0.33	0.04	0.24	0.29	-0.59
JT-60U	34487	-0.11	0.12	–	-0.15	-0.14	–	-0.09	-0.11	–	–
JT-60U	39056	-0.14	0.07	–	-0.13	0.19	–	-0.02	0.16	–	–
DIII-D	87031	0.22	0.32	0.33	0.11	-0.02	0.54	0.03	0.12	0.33	-0.05
DIII-D	95989	-0.07	0.39	0.55	-0.02	0.09	0.76	0.26	-0.05	0.21	-0.13

Table 3: The standard deviations of the simulation predictions with the Bohm/GyroBohm model $\sigma_{\mathrm{Y,B}}$, with the Weiland model $\sigma_{\mathrm{Y,W}}$ and with the GLF23 model $\sigma_{\mathrm{Y,G}}$, including the subtracted mean $m_{\mathrm{Y},i}$.

Tokamak	Pulse No.	$\sigma_{\mathrm{Ti,B}}$	$\sigma_{\mathrm{Ti,W}}$	$\sigma_{\mathrm{Ti,G}}$	$\sigma_{\mathrm{Te,B}}$	$\sigma_{\mathrm{Te,W}}$	$\sigma_{\mathrm{Te,G}}$	$\sigma_{\mathrm{ne,B}}$	$\sigma_{\mathrm{ne,W}}$	$\sigma_{\mathrm{v_\phi,B}}$	$\sigma_{\mathrm{v_\phi,W}}$
JET	46664	0.11	0.22	0.56	0.15	0.06	0.69	0.11	0.09	0.33	0.26
JET	53521	0.23	0.17	0.25	0.11	0.20	0.36	0.16	0.18	0.35	0.24
JT-60U	34487	0.12	0.39	–	0.05	0.06	–	0.05	0.07	–	–
JT-60U	39056	0.12	0.19	–	0.09	0.27	–	0.17	0.31	–	–
DIII-D	87031	0.25	0.60	0.42	0.08	0.23	0.43	0.22	0.19	0.54	0.29
DIII-D	95989	0.18	0.79	0.72	0.15	0.26	0.56	0.36	0.07	0.32	0.39

The accuracy of the simulation predictions can be evaluated in many ways. One of the most crucial points is whether one prefers the simulation results to agree with the experimental results at one instant (typically at the end of the simulation) or throughout the simulation. In the case of ITB formation and non-stationary plasmas during the simulation, as in this study, the best way to eval-

uate the goodness of the model performance is the latter option. However, then the interpretation of the modelling offsets and standard deviations is not straightforward. Still, as a general rule one can apply that if the standard deviation with a subtracted mean is small, the agreement with respect to the location and strength of the ITB is good, provided that the offset is also small. A small time averaged modelling offset or a rather small standard deviation alone does not necessarily imply a good agreement.

There are several conclusions to be drawn from tables 2 and 3. The standard deviations are clearly smaller in JET and JT-60U than those in DIII-D, in particular with the Bohm/GyroBohm model. This can be interpreted that the main mechanisms in the transport model (s, $\omega_{\mathrm{E\times B}}$ and α-stabilisation) that govern the dynamics of the ITB might be different or playing different roles in DIII-D from those in JET and JT-60U. After including the α-stabilisation in the model, the difference in the modelling accuracy between DIII-D and JET or JT-60U decreased, in particular in the ion heat and toroidal velocity transport channels. Still, the prediction accuracy is slightly worse in DIII-D. One reason for the dissimilar behaviour of the ITBs predicted by the model could be the geometry and size of DIII-D that differ from those in JET and JT-60U significantly. Moreover, the toroidal rotation profile is qualitatively different and thus may affect the dynamics of the ITBs in a different way. There is evidence that different numerical factors multiplying the $\omega_{\mathrm{E\times B}}$ flow shear, which comes partly from the toroidal rotation profile, are needed in transport modelling between JET and DIII-D [3].

Another conclusion is that the agreement between the simulations with the Bohm/GyroBohm model and experiments is better in plasmas with a flat q-profile than with a reversed one. This may be an indication that the turbulence suppression by the negative magnetic shear is different than predicted by the model in equation 5. One way to modify this is to include some magnetic shear dependence in GyroBohm term in equation 4. However, adding a factor like $s/(s+1)$ into equation 4 has only a very minor impact on the plasma profiles because the GyroBohm term contributes generally less to the total χ_{i} and χ_{e} than the Bohm term.

By comparing the predictions with the Bohm/GyroBohm model between the different transport channels one can conclude that the electron heat channel is best reproduced. The ion heat and particle transport channels still fall typically within the category of acceptable prediction accuracy whereas the toroidal rotation is beyond the reasonable accuracy. In the case of the Weiland model, the agreement between the experiments and simulations is poorest in the ion heat and toroidal rotation transport channels. This is probably because of more clear ITBs appearing in those two channels due to the dominant ion heating. According to the statistical analysis, in order to best improve the predictive capability of both the Bohm/GyroBohm and Weiland transport models in ITB plasmas, understanding of the momentum transport, i.e. the role of anomalous viscosity must be increased.

As a consequence of weighing the location and strength of the ITB in the statistical analysis, the mean and standard deviation are large with GLF23 because it underestimates the location of

the ITB. What is remarkable is that GLF23 is the only transport model that predicts the ion heat transport better than the electron heat transport.

5. SUMMARY AND CONCLUSIONS

The predictive capabilities of three transport models, Bohm/GyroBohm, Weiland and GLF23, have been investigated in ITB plasmas from the ITPA ITB database. The main emphasis in the transport model evaluation was on the prediction accuracy of the radial location and strength of the ITB. The experimental data from the ITPA ITB database provided the basis for performing the multi-tokamak transport model comparisons. Two discharges from JET, JT-60U and DIII-D were simulated with JETTO and CRONOS transport codes. The fully predictive simulations were carried out for the whole time duration that exists in the ITB database. This is the first time when the ITB/transport models have been tested on three large tokamaks with different q-profiles and in a fully predictive way for $T_{\rm i}$, $T_{\rm e}$, $n_{\rm e}$, q and v_ϕ.

The Bohm/GyroBohm model predicted the location and strength of the ITB as well as the profiles of $T_{\rm i}$, $T_{\rm e}$ and $n_{\rm e}$ within a good accuracy ($\sigma < 0.2$) in JET. This good predictive capability of the Bohm/GyroBohm model in JET was something to be expected because the ITB threshold condition, $0.1 + s - \omega_{\rm E\times B}/\gamma_{\rm ITG} < 0$, was derived using the ITB discharges from JET [8]. On the other hand, it was derived using only ITB discharges with zero or positive magnetic shear and therefore, it could have been not applicable to plasmas with a negative shear. Thus, this study has been a thorough test of the model because there were pulses from three tokamaks and moreover, one discharge from each tokamak had a negative magnetic shear.

What was more astonishing is that the predictions by the Bohm/GyroBohm model with the same ITB formation condition were in better agreement with the experiments in JT-60U than in JET. The standard deviations of $T_{\rm i}$, $T_{\rm e}$ and $n_{\rm e}$ profiles were smaller on average in JT-60U than in JET. In addition, the balanced NBI in JT-60U creates almost no toroidal rotation, causing the $\omega_{\rm E\times B}$ shearing rate to be born from the pressure gradient and poloidal rotation whereas in JET the main contributor to the $\omega_{\rm E\times B}$ shearing rate is the toroidal rotation. Nevertheless, despite the differences in NBI, geometry, plasma current and heating power between the JET and JT-60U discharges, the empirical ITB threshold condition seems to work very well in both tokamaks.

The agreement of the predictions by the Bohm/GyroBohm model was not as good in DIII-D as in JET or JT-60U. The radial location of the ITB was overestimated approximately by $\rho \approx 0.10$–0.15 and the model did not predict the peaking of $T_{\rm i}$ and v_ϕ towards the axis. Therefore, the ITB formation threshold condition was modified to include the effect of the α-stabilisation, as shown in equation (12). This modified ITB threshold condition reproduced the location of the ITB and the shape of the plasma profiles significantly better than the ITB condition without the α-stabilisation in DIII-D. In JET and JT-60U, the difference between the simulations with and without the α-stabilisation term was less than 10 %. Since after including the α-stabilisation the predicted ITBs shrank in DIII-D, but not in JET and JT-60U, the α-stabilisation has a weaker effect

on ITBs, at least around the footpoint of the ITBs, in DIII-D than in JET and JT-60U. However, from the modelling point of view, in order to reach a good agreement between the modelling and experiments in DIII-D, the inclusion of the α-stabilisation explicitly in the ITB formation threshold condition, together with the modified value of constant C_1, was crucial. This can be interpreted that in JET and JT-60U, the effect of α can be hidden, possibly by coincidense, in the value of constant C_1 while in DIII-D, α must be taken explicitly as a separate contributor to the ITB formation threshold condition. In conclusion, the best agreement with the Bohm/GyroBohm transport model in the multi-tokamak ITB database is achieved when the α-stabilisation is taken explicitly into account, as shown in equation (12), rather than hidden into the value of constant C_1.

The Weiland model is not capable of predicting the behaviour of the ITB plasmas satisfactorily in the multi-tokamak database. It did not predict a clear ITB for any of the simulated discharges. Because of this, it tended to underestimate the central ion temperature. The electron temperature and density were better reproduced, the standard deviations were smaller in those channels than in the ion heat transport channel. This is probably due to the dominant ion heating among the simulated discharges. The main reason for the failure of the Weiland model seemed to be the oversize growth rates of the unstable modes (ITG,TEM,...), calculated by the model. The growth rates exceeded the $\omega_{\mathrm{E\times B}}$ shearing rate by a factor of 2–10, thus preventing the ITBs from forming. The growth rates predicted by the Weiland model exceeded those predicted by KINEZERO by a factor of 2–3. However, qualitatively both codes gave the same type (ITG, TEM) for the leading micro-instability for each discharge. In addition, the Weiland model predicted unstable modes up to $\rho = 0.1 - 0.2$ whereas KINEZERO predicted unstable modes typically outside $\rho = 0.4$. Earlier simulations with the Weiland model showed a way to decrease or stabilise the growth of the modes, in particular ITG, as having plasmas with short density gradient lengths [16]. However, the simulated discharges had all a relatively flat density profile, making the turbulence stabilisation by the density gradient rather inefficient. In addition, there are indications that taking into account the electro-magnetic effects, collisions and modifying the dependence of the growth rates on the magnetic shear leads towards better agreement of the Weiland model in ITB plasmas.

The GLF23 model predicted the existence of the ITB (in three of the four simulated discharges), unlike the Weiland model, but the footpoint of the ITB was located too far inside the plasma. This was due to the growth rates exceeding marginally the $\omega_{\mathrm{E\times B}}$ shearing rates. As a result, the prediction for the central temperatures was always underestimated. This suggests that some adjustments of the turbulence stabilisation mechanisms are necessary in the model, in view of triggering broader ITBs. A distinctive and remarkable feature of GLF23 is the very good agreement of its temperature predictions outside the ITB, often even better than that predicted by the Bohm/GyroBohm model. This shows that GLF23 predicts the correct level of anomalous heat transport in the absence of a strong local turbulence stabilisation.

In general, as shown clearly by the statistical analysis in section 4, the most difficult transport channel to predict was the toroidal rotation. The Weiland model in particular had significant

problems in reproducing the experimental toroidal velocity profiles. However, as toroidal rotation profile is strongly, non-linearly linked to ITB formation and dynamics via the $\omega_{\mathrm{E}\times\mathrm{B}}$ shearing rate, an accurate prediction for v_ϕ is crucial. As a consequence, momentum transport is one of the key areas where increased understanding can lead to significantly improved prediction accuracy in ITB plasmas.

The interesting question to be raised is how reliably we can predict the behaviour of the ITB plasmas in future devices, for example in ITER. The semi-empirical Bohm/GyroBohm with its ITB formation threshold condition was derived empirically from JET ITB plasmas. Although it works very well in JET and in a similar size tokamak (JT-60U) and also in a smaller size tokamak (DIII-D) when including the α-stabilisation, it does not prove that the same modelling capability and accuracy can be extrapolated to much larger size tokamaks. On the other hand, the predictions with the first-principle transport models, the Weiland and GLF23, are not in a satisfactory agreement even with the experimental results from the present tokamaks. In addition, from the modelling and scenario development point of views, an ITB/transport model must be able to predict the time evolution of ITB plasmas under a varying q-profile, not just be able to predict a stationary ITB at one time slice. As a consequence, the predictions of these models in ITB plasma scenarios in ITER cannot be regarded as reliable enough for the time being. This is a real problem for the development of advanced tokamak scenarios for ITER, where a proper alignment between the ITB and non-inductive current is critical for steady-state operation [40]. Whether this alignment can be reached or not, depends strongly on the coupling mechanisms between the pressure and current profiles, among them all those underlying the ITB physics. Therefore, future efforts must be further directed towards clarifying the role of different stabilisation mechanisms ($\omega_{\mathrm{E}\times\mathrm{B}}$ shearing rate, magnetic shear, α-stabilisation, role of rational q surfaces, ...), as well as the magnitude of turbulence suppression within the ITB. And finally that physics should be implemented into a reliable first-principle transport model, in view of developing advanced tokamak scenarios for steady-state operation in ITER.

ACKNOWLEDGEMENTS

This work has been conducted under the European Fusion Development Agreement. The authors are grateful to the ITPA Topical Group on Transport Physics for initialising this study and giving access to the ITPA ITB database. The authors also like to thank Jon Kinsey for his advice on using the GLF23 transport model.

REFERENCES

[1] Connor J W *et al.* 2003 *Plasma Phys. Control. Fusion* **45** 455.

[2] Connor J W *et al.* 2004 *Nucl. Fusion* **44** R1.

[3] Zhu P, Bateman G, Kritz A H and Horton W 2000 *Phys. Plasmas* **7** 2898.

[4] Gohil P *et al.* 2003 *Nucl. Fusion* **43** 708.

[5] Parail V V *et al.* 1999 *Nucl. Fusion* **39** 429.

[6] Fukuda T *et al.* 2001 *Proc. 28th European Physical Society Conf. on Controlled Fusion and Plasma Physics (Madeira, Portugal, 18–22 June, 2001) (ECA vol 25A)*, P-5.115.

[7] Burrell K H *et al.* 1997 *Phys. Plasmas* **4** 1499.

[8] Tala T J J *et al.* 2001 *Plasma Phys. Control. Fusion* **43** 507.

[9] Shirai H *et al.* 2000 *Plasma Phys. Control. Fusion* **42** A109.

[10] Gohil P *et al.* 2003 *Plasma Phys. Control. Fusion* **45** 601.

[11] Beer M A, et al. 1997 *Phys. Plasmas* **4** 1792.

[12] Staebler G M *et al.* 1998 *Plasma Phys. Control. Fusion* **40** 569.

[13] Ide S *et al.* 2002 *Plasma Phys. Control. Fusion* **44** A137.

[14] Bourdelle C *et al.* 2003 *Proc. 30th European Physical Society Conf. on Controlled Fusion and Plasma Physics (St. Petersburg, Russia, 7–11 July, 2003) (ECA vol 27A)*, P-1.89.

[15] Staebler G M 1999 *Nucl. Fusion* **39** 815.

[16] Tala T J J *et al.* 2002 *Plasma Phys. Control. Fusion* **44** A495.

[17] Joffrin E *et al.* 2002 *Nucl. Fusion* **42** 235.

[18] Garbet X *et al.* 2001 *Plasma Phys. Control. Fusion* **43** A251.

[19] Erba M *et al.* 1997 *Plasma Phys. Control. Fusion* **39** 261.

[20] Weiland J *Collective Modes in Inhomogeneous Plasma* Institute of Physics Publishing, Bristol 2000.

[21] Strand P, Nordman H, Weiland J and Christiansen J 1998 *Nucl. Fusion* **38** 545.

[22] Waltz R E *et al.* 1997 *Phys. Plasmas* **4** 2482.

[23] Waltz R E and Miller R 1999 *Phys. Plasmas* **6** 4265.

[24] Bourdelle C *et al.* 2002 *Nucl. Fusion* **42** 892.

[25] Bourdelle C *et al.*, this journal.

[26] Basiuk V *et al.* 2003 *Nucl. Fusion* **43** 822.

[27] Houlberg W A *et al.* 1997 *Phys. Plasmas* **4** 3231.

[28] Genacchi G, and Taroni A 1988 JETTO: A free boundary plasma transport code (basic version), *Rapporto* ENEA RT/TIB 1988(5).

[29] Maget P *et al.* 2003 *Plasma Phys. Control. Fusion* **45** 1385.

[30] Hahm T S and Burrell K H 1995 *Phys. Plasmas* **2** 1648.

[31] Ohkawa T 1978 *Phys. Lett. A* **67** 35.

[32] de Esch H P L, Stork D, Weisen H 1990 *(Proc. 17th European Physical Society Conf. on Controlled Fusion and Plasma Physics (Amsterdam, The Netherlands, 25–29 June, 1990) (ECA vol 14B)* p 90.

[33] Jarmen A, Andersson P and Weiland J 1987 *Nucl. Fusion* **27** 941.

[34] Nordman H, Weiland J and Jarmen A 1990 *Nucl. Fusion* **30** 938.

[35] Weiland J and Hirose A 1992 *Nucl. Fusion* **32** 151.

[36] Maget P *et al.* 1999 *Nucl. Fusion* **39** 2063.

[37] Baranov Yu *et al.* 2004 *Plasma Phys. Control. Fusion* **46** 1181.

[38] Dimits A M *et al.* 2000 *Phys. Plasmas* **7** 969.

[39] Kinsey J E *et al.* 2002 *Phys. Plasmas* **9** 1976.

[40] Taylor T S 1997 *Plasma Phys. Control. Fusion* **39** B47.

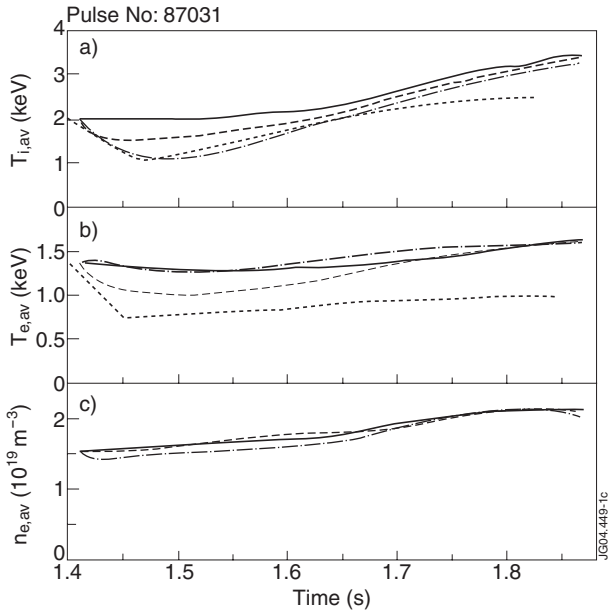

Figure 1: Time traces of the volume averaged ion temperature (a), electron temperature (b) and electron density (c) for DIII-D Pulse No: 87031. The solid lines correspond to the experimental data and the dashed, dash-dotted and dotted lines to the predictions by the Bohm/GyroBohm, Weiland and GLF23 transport models, respectively.

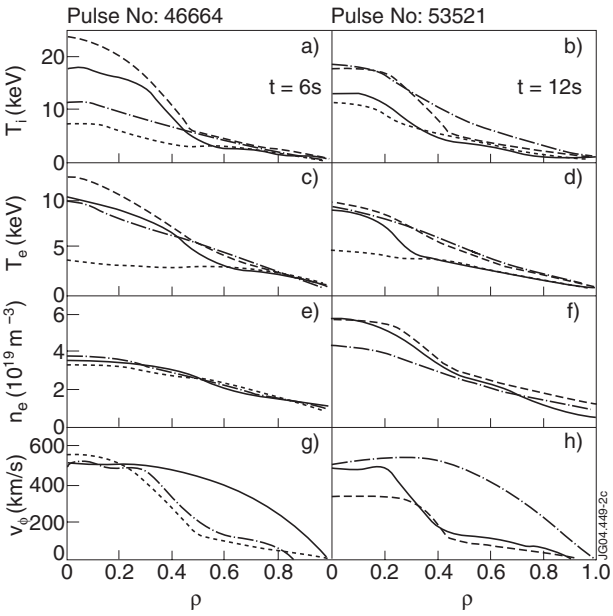

Figure 2: Profiles of the ion temperature (a) and (b), electron temperature (c) and (d), electron density (e) and (f) and toroidal rotation (g) and (h) for JET Pulse No's: 46664 at t=6.0 s (left-hand side) and 53521 at t=12.0 s (right-hand side). The solid lines correspond to the experimental data and the dashed, dash-dotted and dotted ones to the predictions by the Bohm/GyroBohm,Weiland and GLF23 transport models, respectively.

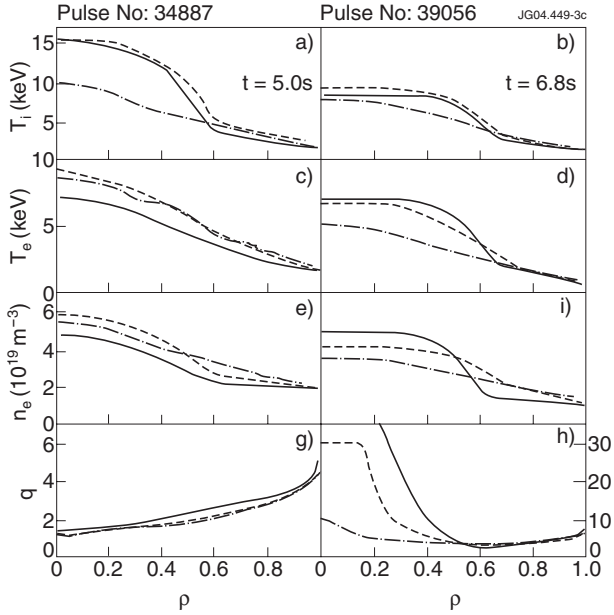

Figure 3: As in figure 2, but for JT-60U Pulse No's: 34487 at t=5.0 s (left-hand side) and 39056 at t=6.8 s (right-hand side). In addition, v_ϕ is replaced with q in (g) and (h).

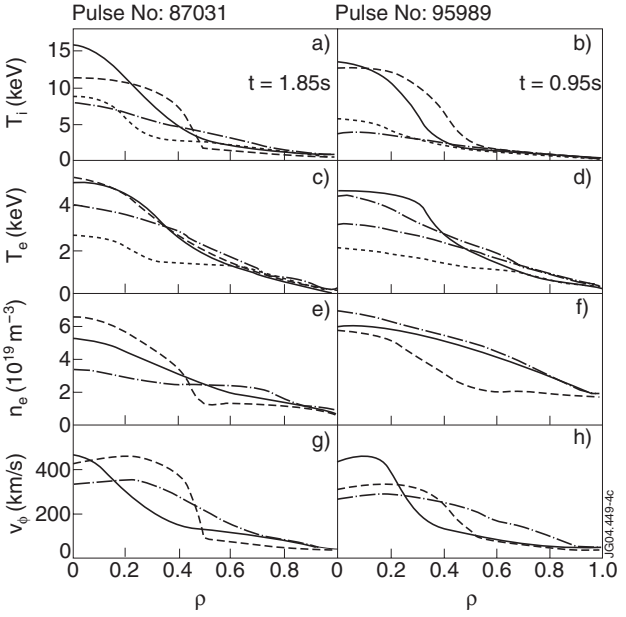

Figure 4: As in figure 2, but for DIII-D Pulse No's: 87031 at t=1.85 s (left-hand side) and 95989 at t=0.95 s (right-hand side).

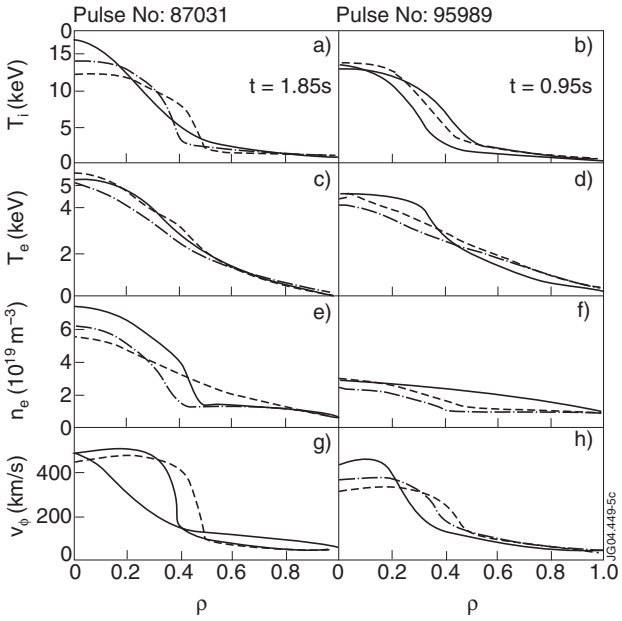

Figure 5: As in figure 4 (solid is the experiment and dashed the prediction by the Bohm/GyroBohm model), but now the dash-dotted lines correspond to the predictions with the amended ITB model including the stabilisation.

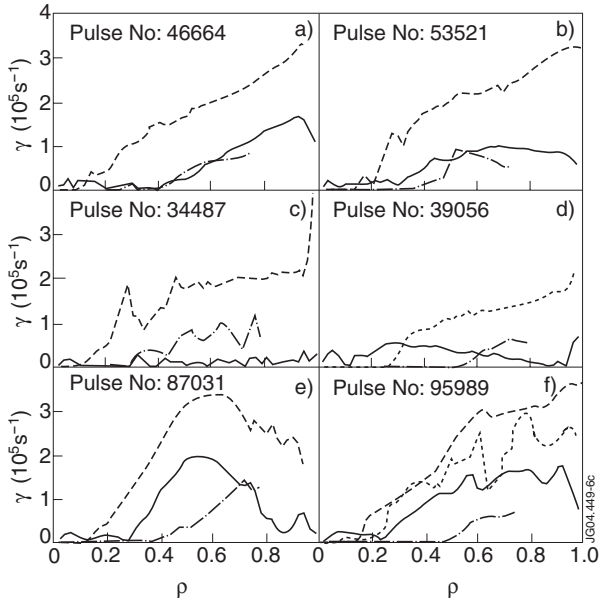

Figure 6: The $\omega_{E\,x\,B}$ shearing rates (solid lines) and the linear growth rates(dashed lines) calculated by the Weiland model for JET Pulse No's: 46664 (a) and 53521 (b), JT-60U discharge no. 34487 (c) and 39056 (d) and DIII-D discharge no. 87031 (e) and 95989 (f). The dash-dotted lines present the growth rates calculated with kinezero. The dotted line in (f) shows the growth rate when the electro-magnetic effects and collisions are taken into account in the Weiland model. The times of the micro-stability analysis correspond to those in figures 2–4 for each discharge, respectively.

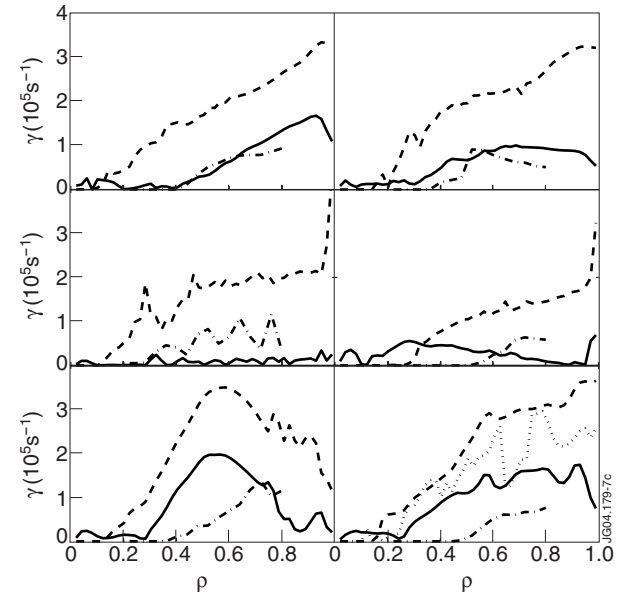

Figure 7: The $\omega_{E\,x\,B}$ shearing rates (solid lines) and the linear growth rates of the fastest growing mode (dashed lines) calculatedby the GLF23 model for JET Pulse No's: 46664 (a) and 53521 (b) and DIII-D Pulse No's: 87031 (c) and 95989 (d). The timesof the micro-stability analysis correspond to those in figures 2 and 4 for each discharge, respectively.